Chemosphere 349 (2024) 140888

Contents lists available at ScienceDirect

Chemosphere

journal homepage: www.elsevier.com/locate/chemosphere

Ozonation using a stainless-steel membrane contactor: Gas-liquid mass transfer and pharmaceuticals removal from secondary-treated municipal wastewater

María A. Prada-Vásquez [a,b,c], Mateus Mestriner Pituco [c,d], Mateus P. Caixeta [c,d], Santiago A. Cardona Gallo [a], Ana M. Botero-Coy [e], Félix Hernández [e], Ricardo A. Torres-Palma [b], Vítor J. P. Vilar [c,d,*]

[a] Universidad Nacional de Colombia, Sede Medellín, Facultad de Minas, Departamento de Geociencias y Medioambiente, Medellín, Colombia
[b] Grupo de Investigación en Remediación Ambiental y Biocatálisis (GIRAB), Instituto de Química, Facultad de Ciencias Exactas y Naturales, Universidad de Antioquia UdeA, Calle 70 No. 52-21, Medellín, Colombia
[c] LSRE-LCM – Laboratory of Separation and Reaction Engineering-Laboratory of Catalysis and Materials, Faculty of Engineering, University of Porto, Rua Dr. Roberto Frias, 4200-465, Porto, Portugal
[d] ALiCE – Associate Laboratory in Chemical Engineering, Faculty of Engineering, University of Porto, Rua Dr. Roberto Frias, 4200-465, Porto, Portugal
[e] Environmental and Public Health Analytical Chemistry, Research Institute for Pesticides and Water, University Jaume I, Castelló, Spain

HIGHLIGHTS

- O_3-liquid mass transfer enhancement provided by stainless-steel membrane contactor.
- K_La values up to 3 times higher than those obtained in a traditional bubble column.
- Liquid and gas flow rate have a major impact on the ozone mass transfer.
- 80% removal for 12 of the 23 PhACs at very short contact times.
- Linear correlation between UV_{254} reduction and specific ozone dose.

GRAPHICAL ABSTRACT

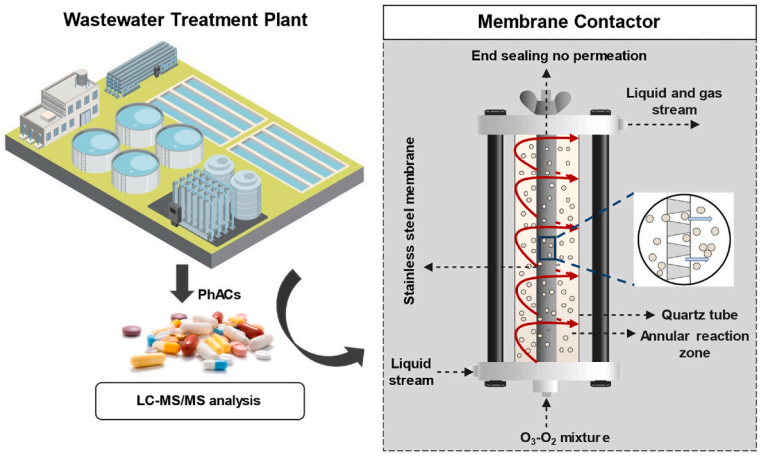

ARTICLE INFO

Handling editor: E. Brillas

ABSTRACT

A tubular porous stainless steel membrane contactor was characterized in terms of ozone-water mass transport, as well as its application in removing 23 pharmaceuticals (PhACs) detected in the secondary-treated municipal wastewater, under continuous mode operation. The volumetric mass transfer coefficient (K_La) was evaluated

* Corresponding author. LSRE-LCM – Laboratory of Separation and Reaction Engineering-Laboratory of Catalysis and Materials, Faculty of Engineering, University of Porto, Rua Dr. Roberto Frias, 4200-465, Porto, Portugal.
E-mail address: vilar@fe.up.pt (V.J.P. Vilar).

https://doi.org/10.1016/j.chemosphere.2023.140888
Received 18 October 2023; Received in revised form 1 December 2023; Accepted 2 December 2023
Available online 7 December 2023

Keywords:
Ozone membrane contactor
Contaminants of emerging concern
Ozone gas/water mass transfer
Wastewater treatment
Ozonation

based on liquid flow rate, gas flow rate, and ozone gas concentration. The K_La values were substantially improved with an increment in liquid flow rate (1.6 times from 30 to 70 $dm^3\ h^{-1}$) and gas flow rate (3.6 times from 0.30 to 0.85 $Ndm^3\ min^{-1}$) due to the improved mixing in the gas-liquid interface. For the lowest liquid flow rate (30 $dm^3\ h^{-1}$), the water phase boundary layer (82%) exhibited the major ozone transfer resistance, but it became almost comparable with membrane resistance for the highest liquid flow rate (70 $dm^3\ h^{-1}$). Additionally, the influence of the specific ozone dose (0.39, 0.53, and 0.69 g O_3 g DOC^{-1}) and ozone inlet gas concentration ($C_{O_3,g,in}$ = 27, 80, and 134 g Nm^{-3}) were investigated in the elimination of 23 PhACs found in secondary-treated municipal wastewater. An ozone dose of 0.69 g O_3 g DOC^{-1} and residence time of 60 s resulted in the removal of 12 out of the 23 compounds over 80%, while 17 compounds were abated above 60%. The elimination of PhACs was strongly correlated with kinetic reaction constants values with ozone and hydroxyl radicals (k_{O3} and $k^{\bullet}_{HO}$), leading to a characteristic elimination pattern for each group of contaminants. This study demonstrates the high potential of membrane contactors as an appealing alternative for ozone-driven wastewater treatment.

1. Introduction

The global population growth and industrialization have contributed to an increasing number of pollutants continually entering water resources, primarily due to human activities. Contaminants of emerging concern (CECs) present in surface water have raised public concern due to their ubiquity, toxicity, and bioaccumulation in the water environment (Patel et al., 2019). Among CECs, pharmaceutically active compounds (PhACs) are one of the most prevalent micropollutants released in water bodies from a variety of sources (Samal et al., 2022). In particular, wastewater treatment plants (WWTPs) are recognized as one of the major hotspots for releasing PhACs and microbial pollution into receiving aquatic ecosystems (Michael et al., 2013; Botero-Coy et al., 2018; Lopez et al., 2022). As most of these compounds are designed to exhibit biological activity, they may adversely affect sensitive aquatic organisms even at extremely low concentration levels (Santos et al., 2010). Hence, suitable tertiary/quaternary treatments must be implemented to improve WWTP depuration capacity and reduce the continuous introduction of these CECs into the aquatic compartments.

For decades, ozonation has become a widely employed technology to eliminate recalcitrant contaminants in water/wastewater attributed to the high oxidative potential of ozone (O_3, E° = 2.07 V vs. SHE–standard hydrogen electrode) (Beltrán, 2004). Once O_3 is dissolved in water, pollutants can generally be oxidized by a direct route with molecular O_3 or through an indirect pathway mostly driven by strong oxidizing agents, such as hydroxyl radicals ($HO^{\bullet}$) (E° = 2.8 V vs. SHE), generated from self-decomposition of ozone (Staehelin and Holgné, 1982).

Water ozonation methods have traditionally been applied injecting the O_3 gas stream into the liquid phase by sparging gas bubbles via gas diffusers (Gottschalk et al., 2010). However, some drawbacks hinder the use of this conventional injection method, such as low gas-liquid mass transfer. Additionally, to ensure a higher dissolution efficiency of O_3 gas in the aqueous phase, large contact tanks are required (Gao et al., 2005; Gottschalk et al., 2010). Recently, membrane contactors for injecting ozone into water have risen as promising methods to overcome these limiting factors (Schmitt et al., 2022). In gas-liquid membrane contactors, the porous membrane acts as a passive barrier between the gas and water phases, separating the two fluids and enabling continuous contact in a stable interfacial area (Pabby and Sastre, 2013). This configuration offers several advantages over traditional reactors. Major benefits include a high volumetric mass transfer efficiency, predictable flow patterns, easy scale-up by modular design, and small reactor footprints (Pines et al., 2005; Schmitt et al., 2022). Moreover, using membrane contactors may minimize operational costs from a reduction in the required ozone dosage (due to the multiple injection points) and a decrease in the requirements for off-gas disposal (John et al., 2022).

Some studies have explored the efficacy of ozone membrane contactors in water treatment for CECs abatement. For instance, Schmitt et al. (2023) tested a polytetrafluoroethylene (PTFE) hollow fiber membrane contactor to promote the ozonation of a sewage fortified with two PhACs. The system showed high removal rates with short residence times (<3 s). Similarly, Stylianou et al. (2018) demonstrated that a ceramic tubular membrane contactor was effective for the treatment of four pollutants in natural surface waters. Recently, Presumido et al. (2022) presented a borosilicate membrane contactor, operated in continuous mode, to enhance gas (ozone)-liquid (water) mass transfer, as well as its application in the elimination of a CECs mixture fortified in demineralized water. The authors reported removal rates exceeding 80% for 13 of the 19 CECs using an O_3 dose of 12 g m^{-3} and a liquid residence time of 3.9 s.

According to our review of the state-of-the-art, further exploration of ozonation processes using membrane contactors for water/wastewater treatment, in particular for the elimination of CECs at realistic concentrations in real effluents, is still required.

This work aims to assess the performance of a stainless-steel membrane contactor for intensifying ozone-water mass transfer and its application in the removal of a broad range of PhACs at realistic concentration levels (ppb: μg L^{-1}) under continuous flow conditions. In this novel configuration, the ozone gas is introduced through the lumen side of the membrane and rapidly transferred to the liquid phase via numerous ozone injection points along the length of the membrane. A spiral motion of the liquid around the shell side of the membrane is enabled by the tangential inlet and outlet of the liquid. This facilitates a more uniform dispersion of the injected gas, enhancing mass transfer and pollutant oxidation (Presumido et al., 2022). The present work was focused on three main aspects: (i) the presence of relevant PhACs in secondary-treated municipal wastewater, (ii) the effect of different operational parameters, including the O_3 gas concentration ($C_{O_3,g,in}$), liquid flow rate (Q_L), and gas flow rate (Q_G) on the volumetric mass transfer coefficient (K_La), and (iii) the abatement of 23 PhACs detected in the secondary-treated municipal wastewater in relation to the specific ozone dose.

2. Material and methods

2.1. Reagents

Potassium indigotrisulfonate ($C_{16}H_7K_3N_2O_{11}S_3$, Sigma-Aldrich) was used to determine the O_3 concentration in the liquid phase. A phosphate-buffered solution (NaH_2PO_4 and H_3PO_4, Sigma-Aldrich) was employed to adjust the pH when needed. All chemical solutions were prepared using a Milli-Q water system (resistance >18.2 MΩ cm^{-1}). Demineralized water (DW) was employed for the cleaning of the membrane contactor and mass transfer trials. All laboratory chemicals were of analytical grade without any further purification. Pharmaceutical reference standards, as well as isotopically labeled internal standards (ILIS), were obtained from LGC Standards and Dr. Ehrenstorfer™.

2.2. Wastewater sampling collection

The effluent sample was collected after the secondary biological treatment from a municipal WWTP located in the North of Portugal. This WWTP provides services to a population of approximately 120,000 equivalent inhabitants. Furthermore, industrial discharges represent

around 17% of the estimated total in the low season, and the remaining 83% corresponds to domestic wastewater. The studied WWTP is mainly composed of preliminary treatment (screening, desanding, and degreasing), primary settling, activated sludge biological treatment, followed by final disinfection using ultraviolet radiation. The sample was collected during one typical day of WWTP operation after secondary treatment and used within the next three days. Table S1 summarizes the main physical and chemical characteristics of the secondary effluent, and their corresponding analytical methods employed are presented in Text S.1.

For PhACs quantification, the samples were preserved at −20 °C in the dark until analysis (details about the quantification of pharmaceuticals can be found in Text S.2 in the supplementary information).

2.3. Membrane contactor

The ozone contactor consists of an exterior quartz tube (outside diameter = 42 mm; internal diameter = 38 mm; length = 200 mm) and a concentric inner tubular membrane made of stainless steel 316L (average pore size = 1 μm; porosity = 21%; outside diameter = 20 mm; internal diameter = 16 mm; membrane thickness = 2 mm; useful length = 187 mm; provided by AmesPore®). This material is known to be an austenitic grade of stainless steel highly ozone-resistant (Sleeper and Henry, 2002). Two movable polypropylene flanges are used to seal the membrane, and the quartz tube ends. The tangential inlet and outlet points located in the flanges allow a helical motion of the liquid in the annular space between both tubes. Ozone-resistant Viton O-rings were employed to guarantee sealed conditions within the reaction unit. The membrane module was supported vertically by a stainless-steel structure. For more details, please see the previous work of V. Vilar research group (Presumido et al., 2022).

2.4. Experimental setup and procedure

The diagram of the experimental setup used for all trials is presented in Fig. 1. A BMT 802 N ozone generator fed with pure oxygen (O_2, 99.995% supplied by Air Liquide) was used to generate the ozone gas stream. The input gas flow rate was modulated by a digital mass flow controller (Alicat Scientific), and the ozone generator power input was adjusted to reach the desired O_3 concentration. An O_3 gas analyzer (BMT 964) was used to measure the O_3 gas concentration in the inlet and outlet gas streams of the membrane reactor. Dissolved O_3 concentration was monitored using the indigo method (Bader and Hoigne, 1982). All trials were conducted in continuous mode, using a single feed water pass through the annular reaction zone (ARZ). The O_3/O_2 gas mixture was fed into the membrane from its lumen side, permeating through its pores structure and being delivered to the ARZ through millions of small-sized bubbles. Meanwhile, the liquid phase was pumped from a 5 L-jacketed glass vessel, coupled to a thermostatic bath for regulating temperature, to the ARZ of the membrane contactor, where O_3 gas-water contacting occurs. In the gas-liquid mass transfer trials, the membrane reactor outlet was connected to the upper inlet of the column (1.5 dm^3, column height of 370 mm and $Ø_{inner}$ = 73 mm) to separate the residual undissolved ozone from the liquid and minimize the liquid residence time inside the column. The water samples were collected in the outlet of the column located at the bottom. For PhACs removal trials, the outlet stream of the membrane contactor was connected to the inlet of the column located at the bottom, where water samples were collected at the upper outlet of the column, to increase the liquid residence time in the system and enhance the interaction of dissolved ozone and PhACs in the liquid bulk. Samples were collected at pre-determined time intervals once steady-state conditions were reached. In the collected samples, residual O_3 concentration was rapidly eliminated by immersing the tube with the water sample in a water bath at 80 °C. The off-gas was collected at the top of the column, passed through the dehumidifier, and directed to the O_3 analyzer. Finally, the remaining gas was vented through the catalytic O_3 destruction system and sequentially to washing bottles containing of 2% KI solution before being released. After each experimental run, the membrane contactor was cleaned by pumping demineralized water through ARZ. The experimental conditions for all tests are

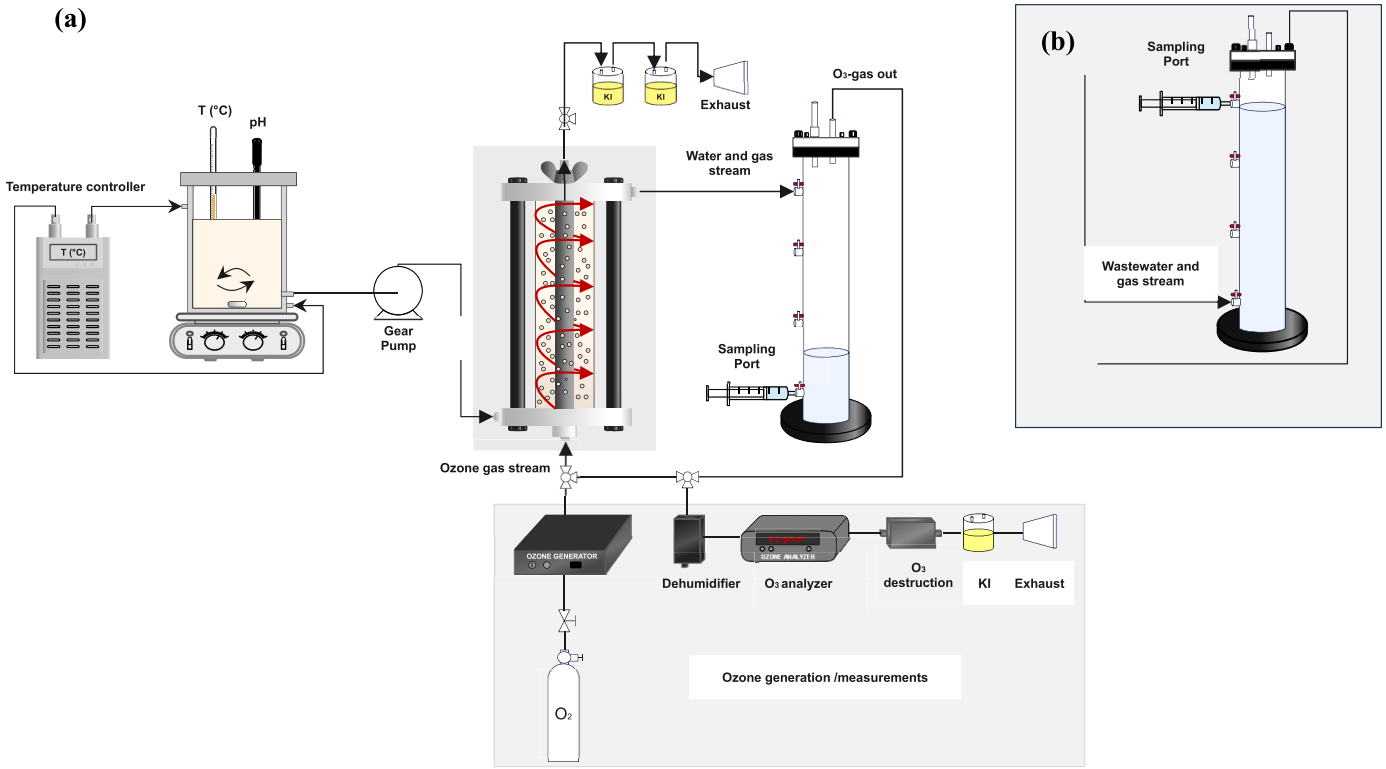

Fig. 1. Diagram of the experimental setup employed for a) experiments on ozone mass transfer and b) for PhACs removal tests.

presented in Table 1.

The estimation of parameters regarding ozone was done at steady-state conditions using the equations presented by Gottschalk et al. (2010) as follows:

Applied ozone dose, AO_3D (g O_3 m^{-3})

$$AO_3D = \frac{Q_G \times C_{O_3,g,in}}{Q_L} \quad (1)$$

Transferred ozone dose, TO_3D (g m^{-3})

$$TO_3D = \frac{(C_{O_3,g,in} - C_{O_3,g,out}) \times Q_G}{Q_L} \quad (2)$$

Consumed ozone dose, CO_3D (g O_3 m^{-3})

$$CO_3D = TO_3D - C_{O_3,l,out} \quad (3)$$

Ozone transfer yield, $\eta(O_3)$ (%)

$$\eta(O_3) = \frac{TO_3D}{AO_3D} \times 100 \quad (4)$$

where $C_{O_3,g,in}$ and $C_{O_3,g,out}$ are the concentration of ozone in the inlet and outlet gas streams (g Nm^{-3}), respectively; $C_{O_3,l,out}$ is the concentration of ozone in the outlet liquid stream; Q_G is the gas flow rate (Ndm^3 min^{-1}) and Q_L (dm^3 h^{-1}) is the liquid flow rate. As the dissolved effluent organic matter (dEfOM) and nitrite (NO_2^-) normally determine the ozone consumption characteristics in wastewater effluents, the transferred O_3 dose was normalized to the dissolved organic carbon (DOC) and corrected to nitrite (NO_2^-) concentration of the secondary effluent (i.e., g O_3/g DOC = g O_3/g DOC - (48/14)(g NO_2^-N/g DOC)) (Lee and Von Gunten, 2016). Thus, the specific transferred O_3 doses were 0.39, 0.53, and 0.69 g O_3 g^{-1} DOC.

2.5. Estimation of ozone mass transfer in the membrane contactor

Ozone mass transfer experiments were conducted using demineralized water at acidic conditions (pH = 2.5) to avoid O_3 decomposition reactions. Initially, the O_3 gas was fed by the lumen side of the membrane, with the shut-off valve fully open, filling the inner space with gas. Following, the water was pumped into the annular zone, and the shut-off valve was closed immediately to allow the permeation of the gas into the liquid side. The concentration of ozone in the off-gas and in the liquid samples collected at the membrane reactor outlet were measured over time until steady-state conditions. A constant temperature of 20 °C was used for all experiments. The effect of various operating parameters in the volumetric mass transfer coefficient, i.e., ozone concentration in the inlet gas stream ($C_{O_3,g,in}$ = 40–80 g Nm^{-3}), liquid flow rate (Q_L = 30–100 dm^3 h^{-1}), and gas flow rate (Q_G = 0.3–0.85 Ndm^3 min^{-1}) was investigated under continuous mode operation.

The two-film theory was adopted to describe the ozone mass transfer, which is usually controlled by the resistance in the liquid phase (Kukuzaki et al., 2010). The volumetric mass transfer coefficient (K_La) (min^{-1}) has been estimated from the mass balance of ozone in the liquid phase, under plug flow conditions, according to Eq. (5).

$$\frac{dC_{O_3,l}}{dt} = K_L a \times \left(C_{O_3^*,l} - C_{O_3,l}\right) - k_d \times C_{O_3,l} \quad (5)$$

where, $\frac{dC_{O_3,l}}{dt}$ (mg dm^{-3} min^{-1}) represents the change of liquid O_3 concentration ($C_{O_3,l}$) over time (t), K_La (min^{-1}) is the product of the O_3 mass transfer coefficient in the liquid phase (K_L) and the interfacial area (a), $C_{O_3^*,l}$ (mg dm^{-3}) is the concentration of O_3 in the liquid in equilibrium with the gas phase, and k_d (min^{-1}) is the rate constant of ozone self-decomposition. Both $C_{O_3^*,l}$ and k_d were measured in semi-batch mode (more details are provided in Text S.3 in the Supplementary material). Under the working conditions of this study, ozone decomposition was negligible, presenting a k_d value of $(115 \pm 7) \times 10^{-4}$ min^{-1} (see Fig S1-a). Therefore, for a continuous mode operation, the integration of Eq. (5) results in Eq. (6), considering the following boundary conditions: $C_{O_3,l} = 0$ at $t = 0$ and $C_{O_3,l} = C_{O_3,l,out}$ at $t = \tau_L$.

$$K_L a = -\frac{1}{\tau_L} \times \ln\left(1 - \frac{C_{O_3,l,out}}{C_{O_3^*,l}}\right) \quad (6)$$

where $C_{O_3,l,out}$ (mg dm^{-3}) is the ozone concentration in the liquid phase at the reactor outlet under steady-state conditions, and τ_L is the liquid residence time, determined by Eq. (7).

$$\tau_L = (1 - \varepsilon_G) \times \frac{V_R}{Q_L} \quad (7)$$

where V_R (dm^3) is the annular zone volume of the membrane reactor (0.166 dm^3), and ε_G is the gas holdup fraction (more details about the

Table 1
Experimental conditions used in the ozone mass transfer tests and in PhACs removal experiments using secondary-treated wastewater.

Ozone mass transfer tests (pH = 2.5, T = 20 °C)							
Parameter	Q_G (Ndm^3 min^{-1})	$C_{O_3,g,in}$ (g Nm^{-3})	Q_L (dm^3 h^{-1})	τ_L (s)	$C_{O_3^*,l}$ [a] (g m^{-3})	$C_{O_3,l,out}$ [a] (g m^{-3})	$K_La_{,20°C}$ (min^{-1})[a]
Q_G	0.30	80	70	8.2	23.5 ± 0.1	4.7 ± 0.06	1.7 ± 0.1
	0.50			8.0		8.3 ± 0.2	3.4 ± 0.2
	0.75			7.5		11.0 ± 0.1	5.3 ± 0.1
	0.85			7.4		12.1 ± 0.2	6.1 ± 0.2
$C_{O_3,g,in}$	0.75	40	70	7.5	9.3 ± 0.03	4.3 ± 0.08	5.2 ± 0.2
		60			16.4 ± 0.02	7.6 ± 0.1	5.1 ± 0.3
		80			23.5 ± 0.1	11.0 ± 0.1	5.3 ± 0.1
Q_L	0.75	80	30	17.5	23.5 ± 0.1	14.0 ± 0.1	3.2 ± 0.3
			50	10.5		12.6 ± 0.1	4.6 ± 0.06
			70	7.5		11.0 ± 0.1	5.3 ± 0.1
			90	5.8		9.21 ± 0.08	5.3 ± 0.4
			100	5.3		8.47 ± 0.09	5.5 ± 0.4

PhACs removal tests (pH = ~7.4, T = ~20–22 °C)								
Test number	Q_L (dm^3 h^{-1})	τ (s)	Q_G (Ndm^3 min^{-1})	$C_{O_3,g,in}$ (g Nm^{-3})	AO_3D (g m^{-3})	TO_3D (g m^{-3})	CO_3D (g m^{-3})	Specific O_3 dose (g O_3 g DOC^{-1})
1	100	60	0.75	20	9	6.3	6.3	0.39
2				27	12	8.6	8.6	0.53
3				40	18	11.0	10.6	0.69
4	100	60	0.25	80	12	10.4	10.4	0.65
5			0.15	134		12.0	11.6	0.73

[a] ± standard error.

experimental procedure for the evaluation of ε_G, interfacial area, and bubble size are provided in Text S.4).

The overall mass transfer resistance, $1/K_L$, was also investigated for the hydrophilic membrane contactor, described as three resistances in series according to Eq. (8) (Kukuzaki et al., 2010).

$$\frac{1}{K_L} = \frac{1}{k_G H} + \frac{1}{k_M} + \frac{1}{k_L} \tag{8}$$

Where k_G, k_M, and k_L are the individual gas phase, membrane, and liquid phase mass transfer coefficients, respectively; $\frac{1}{k_G H}$, $\frac{1}{k_M}$ and $\frac{1}{k_L}$ are the gas, membrane, and liquid mass transfer resistances, respectively; H represents the adimensional Henry's law constant. In a membrane contactor, the mass transfer resistance is controlled by the liquid side during gas-liquid absorption (Johnson and Davis, 1996; Iversen et al., 1997). Since the diffusivity of ozone in gas is 10^4 times greater than liquid phase (Johnson and Davis, 1996), the gas phase mass transfer resistance can be ignored. Thus, Eq. (8) may be rewritten as:

$$\frac{1}{K_L} = \frac{1}{k_M} + \frac{1}{k_L} \tag{9}$$

Details about the calculation of the membrane mass transfer coefficient (k_M) can be found in Text S.5 of the supplementary information.

3. Results and discussion

3.1. Effect of operating conditions on the gas-liquid mass transfer in the membrane contactor

The influence of three parameters on the volumetric ozone mass transfer coefficient, namely the flow rate of the inlet gas and liquid streams, and ozone concentration in the inlet gas stream, was investigated to gain a deeper understanding of the gas-liquid mixing.

3.1.1. Effect of inlet gas flow rate

The ozone mass transfer coefficient was investigated for inlet gas flow rates ranging from 0.30 to 0.85 $Ndm^3\ min^{-1}$, while $C_{O_3,g,in}$ and Q_L were kept at 80 g Nm^{-3} and 70 $dm^3\ h^{-1}$, respectively. As can be seen from Fig. 2a, K_La increased 3.6 times as the Q_G increased from 0.30 to 0.85 $Ndm^3\ min^{-1}$, indicating a considerable influence of gas flow rate in ozone mass transport. This behavior may be attributed to the greater mixing induced by a higher number of bubbles dispersed in the liquid as the inlet gas flow rate increases. As a result, a higher fraction of gas is inside the annular zone, subsequently boosting the liquid velocity in the gas boundary layer (lower liquid residence time inside the reactor). This, in turn, enables a higher driving force for ozone dissolution. In addition, the same principles explain an almost linear correlation between the ozone concentration in the liquid phase at the reactor outlet, at steady state conditions, and the inlet gas flow rate. These findings agree with previous studies regarding the positive influence of gas flow rate on the K_La using ozone membrane contactors (Wang et al., 2021; Presumido et al., 2022). Nevertheless, opposite trends were also observed by other authors, which can be associated with a decrease of the liquid residence time inside the reactor (Bamperng et al., 2010; Berry et al., 2017).

3.1.2. Effect of the ozone concentration in the inlet gas stream ($C_{O_3,g,in}$)

Fig. 2b shows a negligible impact of $C_{O_3,g,in}$ in the K_La values, considering values ranging between 40 and 80 g Nm^{-3}. On the other hand, the ozone concentration in the liquid phase at the reactor outlet under steady-state conditions increased almost proportionally with $C_{O_3,g,in}$, since more O_3 molecules are available in the gas phase (higher partial pressure). As a result, the driving force of the mass transfer is enhanced, leading to larger values of $C_{O_3,l,out}$, in agreement with Henry's law (Sotelo et al., 1989). This trend was also observed by previous authors using membrane contactors (Kukuzaki et al., 2010; Berry et al., 2017; Sabelfeld and Geißen, 2019).

3.1.3. Effect of liquid flow rate

The gas-liquid mass transfer coefficient was evaluated for liquid flow rates varying from 30 to 100 $dm^3\ h^{-1}$ corresponding to Reynolds numbers of 181–604, respectively. As illustrated in Fig. 2c., K_La increased 1.6 times with the liquid flow rate from 30 to 70 $dm^3\ h^{-1}$, and after that, the trend was almost constant. This enhancement is attributed to higher Reynold numbers, enabling diminutive gas bubbles and the potential acceleration of liquid film renewal at the interface, based on thin film renewal theory. This, in turn, develops thinner liquid films, reducing the boundary layer resistance to transfer O_3 into the water phase and enhancing the mass transfer. Additionally, a spiral motion (a swirl) of the water around the membrane shell-side is induced by the inlet and outlet pipes, which are positioned perpendicular to the fluid flow direction and tangentially to the shell, both located at the top on opposite sides in the horizontal plane. This effect is observed when a minimum value of liquid velocity is provided, according to the dimensions of the reactor (Moreira et al., 2019). This leads to a longer effective flow trajectory and enhances the rate of shear on the membrane surface, dragging the gas bubbles from the membrane surface to the bulk (Presumido et al., 2022).

It should be noted that the increase of K_La did not follow a linear trend with Q_L, and the values reached a plateau when Q_L ranged from 70 to 100 $dm^3\ h^{-1}$. This behavior suggests that for Q_L values between 70 and 100 $dm^3\ h^{-1}$, the liquid boundary layer thickness remains similar. Additionally, the membrane resistance also gains an important role in the O_3 mass transfer (see Fig. 3b).

Similar trends have been reported in previous studies, indicating that the volumetric mass transfer coefficient of ozone in water was most significantly affected by changes in liquid flow rate (Pines et al., 2005; Berry et al., 2017; Zoumpouli et al., 2018). However, higher liquid velocities shorten liquid residence time and mainly affect the concentration of dissolved ozone at the reactor outlet. For instance, $C_{O_3,l,out}$ was found to decrease from 14.0 to 8.5 mg L^{-1} when Q_L increased from 30 to 100 $dm^3\ h^{-1}$. Selecting the optimal liquid velocity that ensures a desired level of dissolved O_3 concentration to get an adequate kinetic reaction is a key point.

Moreover, the overall mass transfer coefficient, K_L, was calculated from experimental values of K_La and the gas-water interfacial area (a). It was found that the tubular stainless membrane steel contactor provided an interfacial area in the range of 2054–2841 m^{-1}, with a homogenous distribution of ozone gas bubbles with an average size of 0.25 mm (see Fig. S3). Therefore, K_L values were estimated in the range of 1.9 and 4.5 $\times\ 10^{-5}$ m s^{-1} for Q_L between 30 and 100 $dm^3\ h^{-1}$, respectively.

The investigated gas-liquid membrane contactor showed K_La values in the range of 1.7–6.1 min^{-1}, which are higher than those reported for the conventional bubble columns (K_La ~0.3–1.6 min^{-1}) (Roustan et al., 1996), and slightly lower than venturi injection systems (K_La ~3.6–12.6 min^{-1}) (Roustan, 2003). Nonetheless, in terms of energy consumption, venturi injectors require a higher specific power consumption compared to membrane contactors (Gottschalk et al., 2010; My Hanh Le et al., 2022).

3.1.4. Estimation of membrane transfer coefficient and mass transfer resistances

Mass transfer is not only dominated by the resistance of the liquid boundary film but also by the membrane itself. By using the so-called Wilson plot method (Wilson, 1915), the mass transfer coefficient in the membrane, k_M, was estimated by plotting the experimental data of $1/K_L$ against $1/Q_L$. $1/k_M$ was obtained by the interception of the straight line with the y-axis (where $1/Q_L = 0$, implying $Q_L \rightarrow \infty$ and thus $1/k_L \approx 0$) of the Wilson plot in Fig. 3a. Under the applied experimental conditions, the $1/k_M$ was found to be $(9.74 \pm 0.05) \times 10^3$ s m^{-1}, equivalent to a k_M value of $(1.03 \pm 0.05) \times 10^{-4}$ m s^{-1}.

For a membrane with liquid-filled pores, the mass transfer coefficient can be determined from Eq. (S8), taking into consideration the structural characteristics of the stainless-steel membrane. Based on calculations,

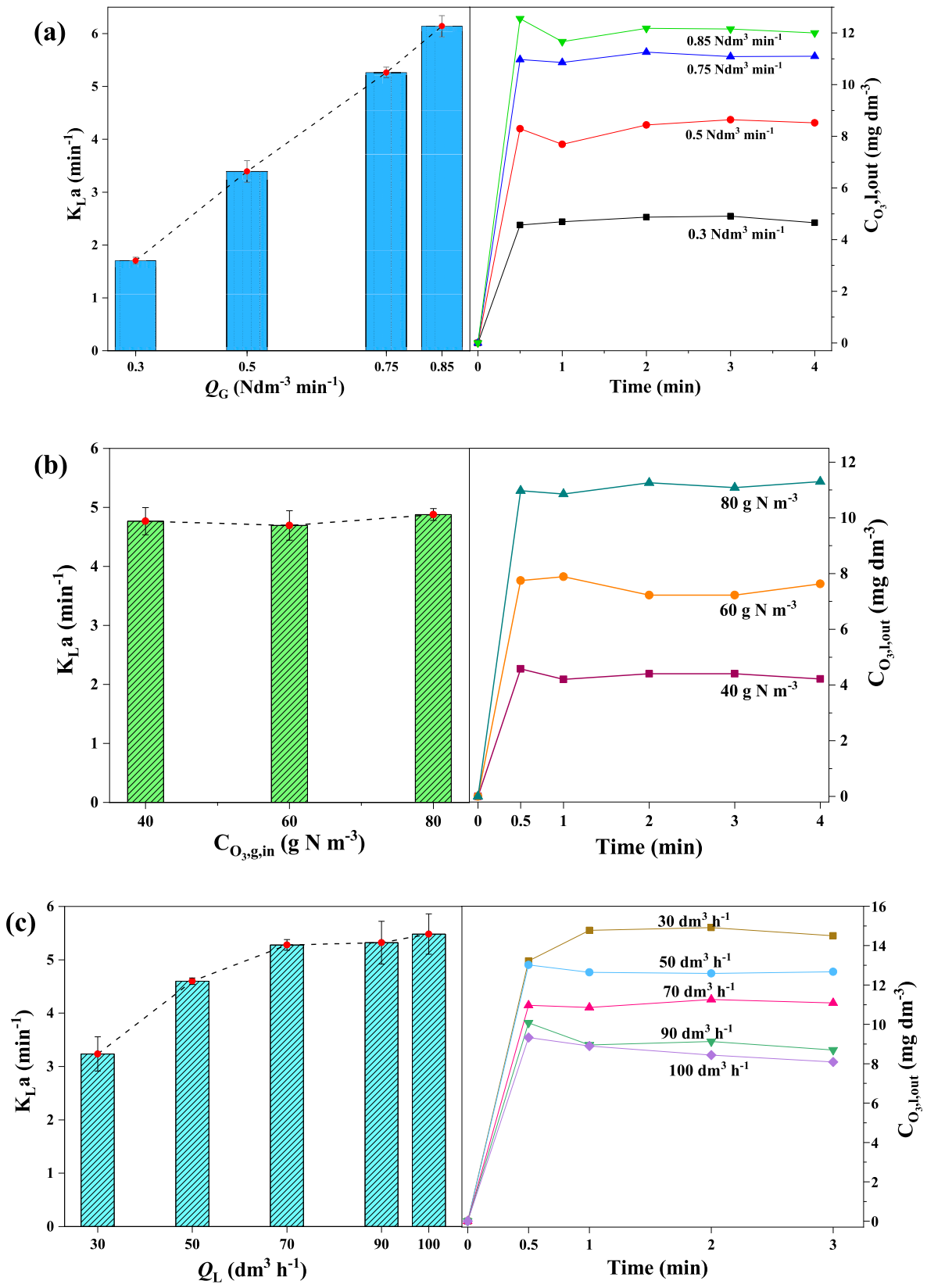

Fig. 2. Effect of the (a) gas flow rate, (b) ozone gas concentration in the inlet stream, and (c) liquid flow rate on K_La values (left side figure) and the dissolved ozone concentration at the membrane reactor outlet (right side figure). Conditions: pH = 2.5, T = 20 °C, (a) Q_L = 70 dm^3 h^{-1}, $C_{O_3,g,in}$ = 80 g Ndm^{-3}, (b) Q_G = 0.75 Ndm^3 min^{-1}, Q_L = 70 dm^3 h^{-1}; (c) Q_G = 0.75 Ndm^3 min^{-1}, $C_{O_3,g,in}$ = 80 g Ndm^{-3}.

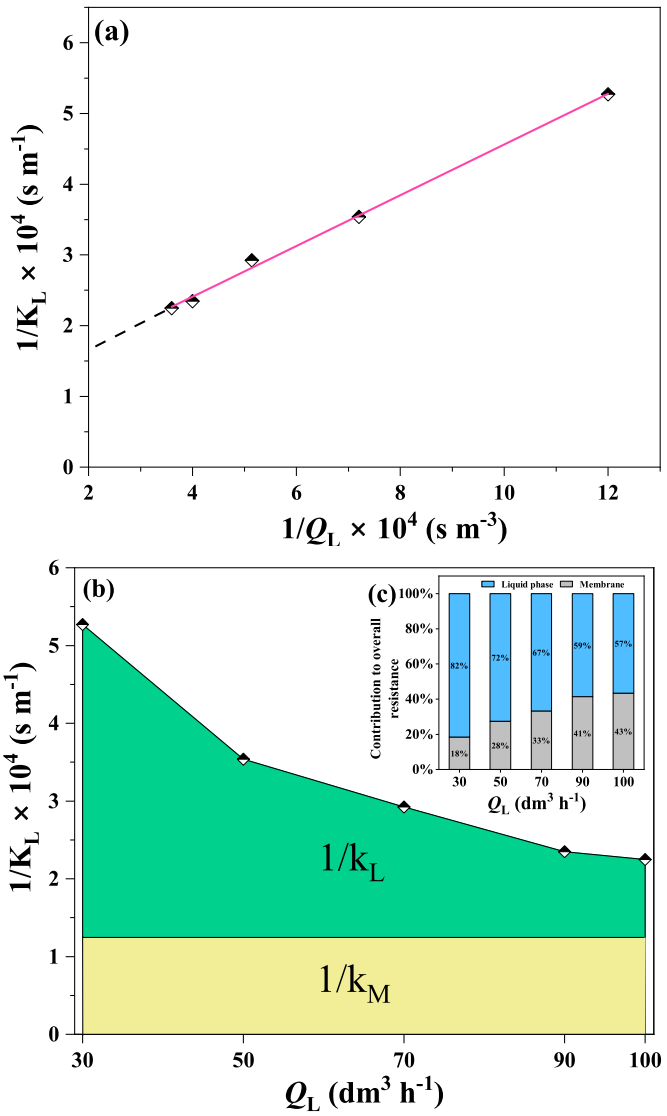

Fig. 3. (a) Graphical scheme for the determination of the mass transfer coefficient in the membrane by Wilson plot method, (b) mass transfer resistances, (c) contribution to total mass transfer resistance (%) in the liquid phase and in the membrane as a function of liquid flow rate. Conditions: Q_L = 30, 50, 70 and 100 dm^3 h^{-1}, $C_{O_3,g,in}$ = 80 mg Ndm^{-3}, Q_G = 0.75 Ndm^3 min^{-1}, pH = 2.5, T = 20 °C.

the theoretical value obtained was $k_M = 2.19 \times 10^{-5}$ m s^{-1}, which exceeds the experimental value, $k_M = (1.03 \pm 0.05) \times 10^{-4}$ m s^{-1} by a factor of 4.7. The possible reason for the large difference between the two values may be attributed to the assumptions considered to obtain Eq. (S8): constant tortuosity, cylindrical pores, and lognormal distribution of the membrane pore size (Kreulen et al., 1993; Lu et al., 2008).

These assumptions probably resulted in an overestimation of the mass transfer resistance through the membrane. Similarly, Khaisri et al. (2010) observed similar results when they studied CO_2 absorption through PTFE hollow fiber membrane contactor. According to the authors, the Wilson plot method produced a more accurate prediction of membrane mass transfer resistance than the theoretical method.

The analysis of the individual mass-transfer resistances in the liquid phase was calculated by substituting the experimental value of K_L and k_M obtained from the Wilson plot method in Eq. (9). Fig. 3b shows the results of individual mass transfer resistances for ozone dissolution at different liquid flow rates. It can be noticed that under conditions of low liquid flow rates (Q_L = 30 dm^3 h^{-1}), the main resistance to O_3 transfer is through the liquid phase boundary layer ($1/k_L$), contributing to 82% of the overall mass transfer resistance (Fig. 3c), with the remaining 18% coming from the membrane. However, when increasing Q_L to 100 dm^3 h^{-1}, the liquid-phase resistance becomes almost comparable with membrane resistance and contributes to 57% and 43% of the overall mass transfer resistance, respectively. Although a higher liquid flow rate can enhance gas transport in the water phase by decreasing the liquid boundary layer resistance, it might also intensify the membrane wetting, which hinders gas transport in the membrane (Khaisri et al., 2009).

The mass transfer resistance is also affected by the material and properties of the membrane (porosity, pore size, and hydrophobicity). Membranes with lower porosity, lower pore size, and a low hydrophobicity exhibit higher resistance to ozone mass transfer (Zhang et al., 2017; Li et al., 2020). As the investigated membrane is hydrophilic, water enters more easily into the pores, increasing the membrane resistance due to the slower diffusion of ozone molecules in water compared to gas (Johnson and Davis, 1996). However, the addition of a hydrophobic layer to the membrane shell-side can be a solution to overcome this limitation (Stylianou et al., 2015).

For similar conditions, the stainless-steel membrane (used in this study) presents a membrane resistance 1.4-fold higher than the borosilicate membrane tested by Presumido et al. (2022). These results may be attributed to the fact that the porosity and mean pore size of the borosilicate membrane used by authors were about 2.0 and 3.8 times greater, respectively, when compared to the stainless-steel membrane investigated in this study. Therefore, as the membrane porosity and pore size increase, higher amounts of ozone gas is able to diffuse through the membrane, decreasing the resistance on the membrane side. Nevertheless, higher pore size can also increase the risk of wetting, reducing the mass transfer (Bakeri et al., 2012). Comparing both membrane contactors, the main disadvantage of the tubular stainless-steel contactor was the higher membrane resistance compared to the borosilicate contactor. This, in turn, resulted in lower $K_L a$ values for this study than those presented by Presumido et al. (2023). However, regarding long-term performance, stainless steel membranes could be a better alternative to be implemented at full-scale due to their higher thermal and mechanical stability (Song et al., 2011).

3.2. Comparison with other gas-liquid contactor systems

A comparison of the performance of the membrane contactor with conventional gas-liquid systems is crucial to assess the degree of process intensification that can be achieved. For the purpose of obtaining a more accurate comparison of the membrane contactor performance with other gas-liquid contactors, the ASCE standards method for measuring oxygen mass transfer was used (ASCE, 2007). In this sense, two parameters were considered: standard oxygen transfer rate (SOTR, kg h^{-1}) and standard oxygen transfer efficiency (SOTE, %). The SOTR is defined as the amount of gas being dissolved per unit of time, while SOTE measures the mass of gas transferred to the liquid phase in relation to the mass of gas supplied to the system. The SORT and SOTE were calculated by Eq. (10) and Eq. (11), respectively, at standard conditions (20 °C water temperature and pressure at 1.013 Pa).

$$SOTR = K_L a_{,O_2} \times C_{O_2^*,l} \times V_R \quad (10)$$

$$SOTE = \frac{K_L a_{,O_2} \times C_{O_2^*,l} \times V_R}{W_{O_2}} \quad (11)$$

where $K_L a_{,O_2}$ refers to the oxygen volumetric mass transfer coefficient (min^{-1}), $C_{O_2^*,l}$ is the dissolved oxygen concentration in equilibrium (9.20 mg L^{-1} (Carvalho et al., 2021)), and W_{O_2} is the mass flow rate of O_2 in the air stream (kg O_2 h^{-1}). W_{O_2} was calculated by assuming that the air behaves as an ideal gas, containing 23 wt% of O_2 at standard conditions.

The $K_L a_{,O_2}$ values were estimated from the O_3 mass transfer coefficients following the surface renewal theory (Beltrán et al., 1998), as

given by the relation in Eq. (12).

$$\frac{K_L a_{,O_3}}{K_L a_{,O_2}} = \sqrt{\frac{D_{O_3}}{D_{O_2}}} = 0.9 \quad (12)$$

where D_{O3} (1.76×10^{-9} m^2 s^{-1}) (Johnson and Davis, 1996) and D_{O2} (2.17×10^{-9} m^2 s^{-1}) (Wilke and Chang, 1955) are the diffusion coefficients of O_3 and O_2 gases in water at 20 °C, respectively.

The SOTR and SOTE values are presented in Table S2 (Supplementary material). It can be seen that the SOTR and SOTE values for traditional injection systems, such as fine bubble diffusers (DeMoyer et al., 2001; Gillot et al., 2005) and venturi injectors (Therrien et al., 2019; Dayıoğlu, 2022) were much higher compared to the membrane contactor. It is important to note that these parameters are strongly influenced by the reactor volume. Hence, the utilization of equipment with greater volumes results in higher values of SOTR and SOTE. For a better comparison, two additional parameters were included: the volumetric SOTR (VSOTR, kg h^{-1} m^{-3}), which was determined by dividing SOTR by the reactor volume, and the second term, the specific SOTE (SSOTE, % m^{-1}), determined by dividing the SOTE by the height of the fluid or water depth (h, m).

From comparable data in terms of VSOTR, the membrane contactor transferred a higher amount of O_2 mass into the water per unit of volume compared to bubble diffusers and venturi injectors. Similarly, regarding the SSOTE efficiency parameter, the membrane contactor achieved an O_2 mass dissolution per unit of reactor height between one to two orders of magnitude greater compared to traditional contactors. This feature make it an appealing device for practical applications in reactions of gas-liquid mass transfer.

On the other hand, although the ASCE method (ASCE, 2007) was initially introduced to describe the oxygen dissolution into water, in this study, both parameters were also extended for the O_3 transfer efficiency (TE, %), as given in Eq. (13). For this case, the mass flow rate of O_3 (W_{O_3}) was determined from the inlet Q_G and $C_{O_3,g,in}$. The TE is an important parameter for setting optimal operation conditions in ozone-based applications (Wang et al., 2023).

$$TE\ (\%) = \frac{K_L a \times C_{O_3^*,l} \times V_R}{W_{O_3}} \quad (13)$$

Fig. S5 shows the transfer efficiency (TE) for O_3 at different Q_L and Q_G calculated based on ASCE standard method. It can be observed that higher Q_L generated higher transfer efficiency values at a fixed Q_G. This characteristic becomes particularly advantageous for large-scale processes in which higher volumes of wastewater need to be treated, such as those produced by municipal WWTPs. On the other hand, for a fixed Q_L, the increase of Q_G developed an almost constant O_3 transfer efficiency. This behavior was probably attributed that the variation of Q_G was small (from 0.50 to 0.85 Ndm^3 min^{-1}) and thus, the efficiency loss remained almost constant for this range of Q_G. It is expected that with higher Q_G (e.g., 0.85 to 2 Ndm^3 min^{-1}) efficacy will decrease, mainly attributed to the shorter contact time between gas−liquid phases.

According to the experimental conditions that used demineralized water with no chemical reaction, the maximum TE of 35% was attained. In this way, considering the O_3 doses required for PhACs abatement in the secondary-treated wastewater, it was selected a Q_G of 0.75 Ndm^3 min^{-1} (second value with highest TE) and a Q_L of 100 dm^3 h^{-1}.

3.3. Pharmaceuticals removal from secondary-treated municipal wastewater

3.3.1. Occurrence of pharmaceuticals

A total of 33 pharmaceuticals were selected for this study based on several criteria, including (i) high consumption rate, (ii) frequency detected in municipal WWTPs, and (iii) their potential risk to the environment (de Jesus Gaffney et al., 2017). The main detected pharmaceuticals and their concentrations are presented in Table 2. Within the pharmaceuticals class, 23 compounds were detected above the limit of quantification (LOQ), belonging to 11 different therapeutic classes: 2 anti-inflammatories, 6 antibiotics, 3 anticonvulsants, 3 antihypertensives, 1 anthelmintic drug, 2 anti-ulcer agents, 1 iodized contrast media, 1 lipid regulator, 1 β-blocker, 2 anxiolytics, and 2 antidepressants. The concentration levels ranged from 0.01 to 1.52 μg L^{-1} (1522 ng L^{-1}), whereas the sum of the pharmaceutical mixture reached a total of 7.31 μg L^{-1}. Among the identified PhACs, the highest average concentrations were found for the non-steroidal anti-inflammatory drug (NSAID) diclofenac (1.52 μg L^{-1}), the iodized contrast media family iopromide (1.04 μg L^{-1}), followed by the antihypertensive irbesartan (0.75 μg L^{-1}), whereas the lowest concentrations values were detected for the anthelmintic levamisole and the anti-ulcer agent pantoprazole (0.01 μg L^{-1}). The level found of diclofenac is correlated to its high consumption in Portugal, presenting the highest share of the over-the-counter drugs market (without no prescription), 18.4% in 2018 (Infarmed, 2018). In relation to antibiotics, fluoroquinolone ciprofloxacin was the antibiotic with the highest concentration detected (0.39 μg L^{-1}), followed by the macrolide clarithromycin (0.13 μg L^{-1}).

Table 2
Concentration of pharmaceuticals detected in the municipal wastewater after secondary treatment.

Therapeutic group	Compound	Concentration (μg L^{-1})
Anti-inflammatory	Diclofenac	1.52
Antibiotics	Ciprofloxacin	0.39
	Clarithromycin	0.13
	Trimethoprim	0.04
	Sulfamethoxazole	0.10
	Clindamycin	0.03
	Norfloxacin	0.09
Anticonvulsants	Carbamazepine	0.51
	Gabapentin	0.68
	Primidone	0.14
Anti-hypertensive	Irbesartan	0.75
	Losartan	0.33
	Valsartan	0.02
Anthelmintic	Levamisole	0.01
Anti-ulcer agents	Pantoprazole	0.01
	4-hidroxy omeprazole sulfide	0.08
Iodized contrast media	Iopromide	1.04
Lipid regulator	Atorvastatin	0.18
Beta-blocker	Metoprolol	0.02
Anxiolytic	Lorazepam	0.11
	Alprazolam	0.01
Antidepressants	Venlafaxine	0.44
	O-desmethylvenlafaxine	0.68
	Total load	7.31

The results obtained in this study are consistent with previous findings reported in European WWTP secondary effluents (de Jesus Gaffney et al., 2017; Lopez et al., 2022; Sá et al., 2022). For instance, de Jesus Gaffney et al. (2017) found diclofenac concentrations ranging between 0.05 and 4.2 μg L^{-1} in Portuguese WWTP secondary effluents. Likewise, the authors detected ciprofloxacin at an average concentration of 0.35 μg L^{-1}.

3.3.2. PhACs removal using the ozone membrane contactor

The performance of the ozonation membrane contactor, operated in continuous mode, in the removal of the 23 PhACs detected in the secondary-treated municipal wastewater was assessed under several specific ozone doses (0.39, 0.53, and 0.69 g O_3 g DOC^{-1}). As shown in Fig. 4a, increasing the ozone doses led to a greater extent of PhACs abatement. At the lowest ozone dose of 0.39 g O_3 DOC^{-1}, only 3 out of the 23 compounds (atorvastatin, clindamycin, and diclofenac) were degraded by over 80%. The low removal may be related to the rapid consumption of ozone by the dissolved effluent organic matter (dEfOM) (Hoigné and Bader, 1994). In fact, ozone was completely consumed within 60 s (system residence time), indicating that the O_3 dose applied

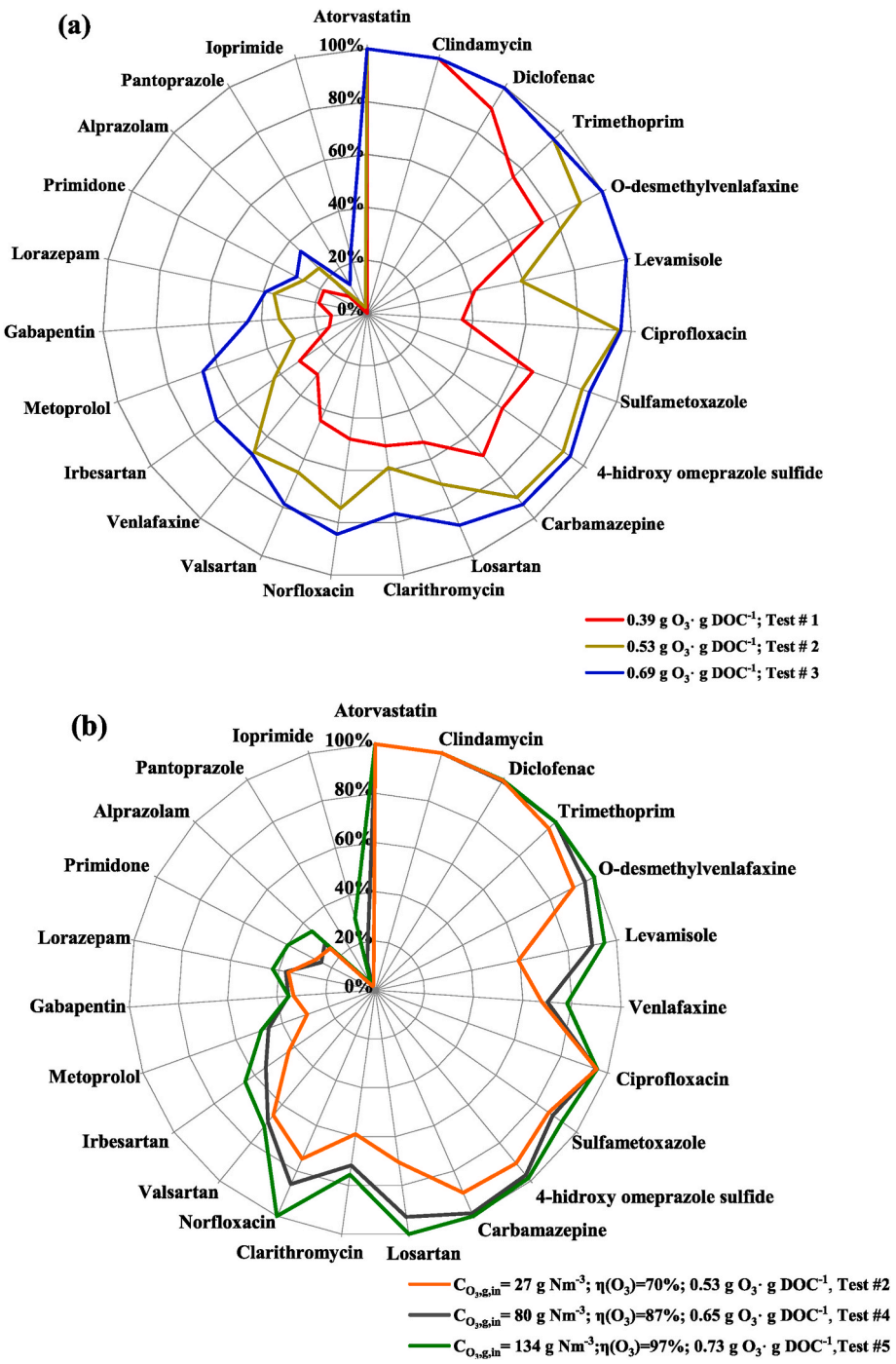

Fig. 4. Removal efficiency for the 23 pharmaceuticals detected in a secondary-treated wastewater, using the membrane reactor coupled with a column, operated in continuous mode ($\tau = 60$ s) as a function of (a) specific ozone doses 0.39, 0.53, and 0.69 g O_3 g DOC^{-1} (the Specific transferred O_3 dose was corrected for nitrite consumption) and (b) O_3 concentration in the inlet gas stream and same AO_3D applied (12 mg O_3 L^{-1}). For more details on the experimental conditions of each test, see Table 2.

is below the Immediate Ozone Demand (IOD). For the intermediate ozone dose, 0.53 g O_3 g DOC^{-1}, 9 compounds (ciprofloxacin, sulfamethoxazole, diclofenac, trimethoprim, clindamycin, atorvastatin, carbamazepine, O-desmethylvenlafaxine - venlafaxine metabolite and 4-hydroxy-omeprazole sulfide - omeprazole metabolite) were eliminated over 80%. These PhACs contain electron-rich moieties (e.g., anilines, olefins, amines, and deprotonated amines), which exhibit a high reactivity for the direct reaction with ozone (Table S4 presents the ozone-reactive moieties for each compound). As shown in Fig. S6-a, the PhACs abatement was strongly correlated with reported second-order rate constants with O_3 (k_{O3}). Compounds that typically exhibit $k_{O3} \geq 10^4$ M^{-1} s^{-1} at circumneutral pH, present removal efficiencies higher than 80% even for low ozone transferred doses (>0.21–1.24 g O_3 g DOC^{-1}) (Zimmermann et al., 2011; Lee and von Gunten, 2012). A similar trend was observed in Fig. S6-a, in which compounds with higher k_{O3} were more quickly eliminated from the wastewater during ozonation.

For the highest specific ozone dose of 0.69 g O_3 g DOC^{-1}, 17 out of the 23 PhACs reached removals of more than ≥60%, of which 12 compounds were abated higher than 80%. Chemical compounds that are

moderately ozone-resistant with k_{O3} between 10^2 and 10^4 M^{-1} s^{-1}, e.g., metoprolol, underwent an increase in elimination level by around 66% or in the case of levamisole which was removed to values lower than the limit of quantification. On the contrary, compounds with low reaction rate with O_3 (k_{O3} <10^2 M^{-1} s^{-1}), such as alprazolam, gabapentin, lorazepam, and primidone, reached low removals (around 30–45%), with particularly low elimination levels for pantoprazole (13%) and iopromide (24%). The low removal of these compounds is related to the presence of carboxylic acid groups (gabapentin), halogen substituents (iopromide, alprazolam), or amides (primidone) that, due to their electron-withdrawing nature, are practically unreactive towards ozone oxidation (Nakada et al., 2007). The free radical HO•, generated from O_3 natural decomposition, plays a crucial role in their abatement during ozonation (Elovitz and Von Gunten, 1999). For ozone-resistant compounds, k_{O3} <10^2 M^{-1} s^{-1}, the main oxidation pathway is the radical-type chain mechanism through HO• radicals. In contrast, for compounds with k_{O3} between 10^2 and 10^4 M^{-1} s^{-1}, a simultaneous ozone molecular and radical mechanism occurs with the same order of magnitude (Lee and Von Gunten, 2016). As depicted in, the degradation efficiency of ozone-resistant compounds (highlighted region in light blue) was also well correlated with their $k_{HO•}$ values. For instance, iopromide with lower HO• reactivity, $k_{HO•}$ <1 × 10^9 M^{-1} s^{-1}, reached the lowest percentage removal compared with the hypertensive compounds such as valsartan and losartan ($k_{HO•}$ > 5 × 10^{10} M^{-1} s^{-1}). There was a weak, non-significant correlation between the removal PhACs, and the three variables: net charge, molecular weight, and solubility (see Fig. S7).

The wastewater matrix components, such as dEfOM and alkalinity (bicarbonates/carbonates, HCO_3^-/CO_3^{2-}), can considerably interfere with the oxidative capacity of radical-based oxidation reactions, due to its scavenging effect over hydroxyl radicals (Lado Ribeiro et al., 2019; Asghar et al., 2022). Given the significantly high concentration of both constituents in the effluent (e.g., mg L^{-1} of DOC and carbonate), a high amount of HO• radicals are consumed by the scavengers, decreasing the PhACs removal capacity by the indirect pathway. Mathon et al. (2021) found for a mixture of 47 CECs present in secondary treated wastewater that, the distribution of HO• consumption was: 0.02% by nitrites and bromides, 11% by bicarbonates, 60% by the sum of all micropollutants, while the remaining 29% was consumed by dEfOM and other chemical species.

Other studies have investigated higher specific ozone doses for the abatement of less reactive compounds with ozone in wastewater (Margot et al., 2013; Lee and Von Gunten, 2016; Guillossou et al., 2020). For instance, Margot et al. (2013) found that even the most ozone-resistant micropollutants were highly removed at an O_3 dose of 2.6 g O_3 g^{-1} DOC, with an average elimination of 80%. However, authors reported that higher ozone doses imply elevated costs, and the generation of toxic by-products is more feasible.

The results presented herein showed similar PhACs abatements using ozone membrane contactors for comparable ozone doses (0.14–0.7 g O_3 g^{-1} DOC) and residence times (2.8–60 s) (Presumido et al., 2023; Schmitt et al., 2023). For instance, Presumido et al. (2023) found removals higher than 80% for up to 13 of the 19 CECs spiked in urban wastewater with an ozone dose of 18 g m^{-3} (1.17 g O_3 g^{-1} DOC) and residence time of 60 s using a borosilicate tubular membrane. On the other hand, compared to conventional processes, the PhACs removal rates achieved in this study were obtained at a very short residence time of 60 s instead of 10–30 min as reported in a conventional process at full WWTP scale (Hollender et al., 2009; Kharel et al., 2020).

Fig. 4b shows the PhACs removal applying the same ozone dose (12 g O_3 m^{-3}) while varying $C_{O_3,g,in}$ (27, 80, and 134 g Nm^{-3}) and Q_G (0.15, 0.25 and 0.75 Ndm^3 min^{-1}) (Table 2). As can be seen, for the highest ozone concentration ($C_{O_3,g,in}$ = 134 g Nm^{-3}, Q_G = 0.15 g Nm^{-3}), 11 out of the 23 compounds reached removals higher than 96% or below the LOQ. This behaviour can be explained according to the mass-transfer theory, in which increasing the ozone-gas input concentration enhances the driving force for O_3 mass transfer from the gas to the water phase (Wang et al., 2019). This, in turn, provides a higher dissolved O_3 concentration enhancing the PhACs removal. Moreover, O_3 transfer yield η(O_3) achieved values near 97% for a $C_{O_3,g,in}$ of 134 g Nm^{-3}, against 70% and 87% for the tests with $C_{O_3,g,in}$ values of 27 g Nm^{-3} and 80 g Nm^{-3}, respectively. These findings demonstrate a favorable characteristic when using the same ozone dose applied to the treatment, as reducing the gas flow rate, and simultaneously increasing the O_3 gas concentration can lead to lower operational costs during ozonation (Al-Abduly et al., 2014).

3.3.3. *Influence of the ozonation process on the global parameters*

The removal of DOC, specific UV absorbance at 254 nm (UV_{254}), and turbidity after ozonation were also investigated as possible control parameters. Fig. 5 illustrates the removal of the mentioned parameters in relation to specific ozone doses and concentrations of ozone in the inlet gas stream.

As can be seen in Fig. 5a, an improvement in DOC removal was attained when increasing the ozone doses. In particular, when applying an O_3 dose of 0.39 gO_3 $gDOC^{-1}$, DOC removal rate was found to be only 3%, whereas an ozone dose of 0.69 g O_3 g DOC^{-1} led to a removal of up to 22%. The highest DOC removal (27%) was achieved for the highest $C_{O_3,g,in}$ (134 g Nm^{-3}) (Fig. 5b). These results confirm the inefficiency of ozonation in organic matter mineralization, with a minimal DOC reduction, even for the highest specific ozone dose tested (Rosal et al., 2008; Marce et al., 2016; Schmitt et al., 2023). Many authors attributed the limited mineralization yield to the generation of persistent organic intermediates that result from the oxidation of dE_fOM initially present in wastewater (Hübner et al., 2015; Iakovides et al., 2019). However, although ozonation does not completely mineralize intermediate products, it can transform them into more biodegradable compounds, which are generally well removed during biological or physical post-treatments (e.g., combined with activated carbon adsorption) (Margot et al., 2013; Völker et al., 2019).

The UV_{254} is a commonly used surrogate parameter to monitor water quality that contains aromatic rings or unsaturated carbon bonds. Therefore, a reduction of the UV_{254} indicates the decomposition of organic compounds into smaller molecules and a change in the aromatic nature of the pollutant (Mecha et al., 2016; Chys et al., 2017). As shown in Fig. 5a, a low reduction in UV_{254} absorbance (22%) was reached with a specific ozone dose of 0.39 g O_3 g DOC^{-1}, while a higher decrease (36%) was obtained for an ozone dose of 0.69 g O_3 g DOC^{-1}. Similar behavior was observed when the highest $C_{O_3,g,in}$ was applied, reaching a reduction of 40% in UV_{254} absorbance (Fig. 5b).

Fig. 5c illustrates the relationship between the percentage of the total PhACs elimination and the decrease in UV_{254} at different specific ozone dosages. Both parameters showed a good correlation (R^2 = 0.996 or based on Pearson correlation ($r_{pearsson}$ = 0.97)), which provided support for the surrogate-based prediction. Overall, a UV_{254} decrease of 36% corresponds to a total PhACs elimination of 74%. Previous studies have also demonstrated that UV_{254} decrease can be correlated with the abatement of individual CECs (Gerrity et al., 2012; Wittmer et al., 2015; Chys et al., 2017).

A linear correlation between the specific ozone dose (SOD) and UV_{254} reduction (UV_{254} reduction = 54 × SOD) can be helpful to allow better monitoring, applying online UV_{254} measurements, of the ozonation process to meet their specific treatment requirements.

Finally, a reduction in the turbidity of the treated effluent was observed, achieving efficiency values of 51% and 65% with the increase of the specific ozone dosage from 0.39 to 0.69 g O_3 g DOC^{-1}, respectively. Marce et al. (2016) observed that ozone destroys the solid particles of organic matter, especially during the initial stage of the reaction when low ozone doses are transferred. This could explain the rapid decrease in turbidity.

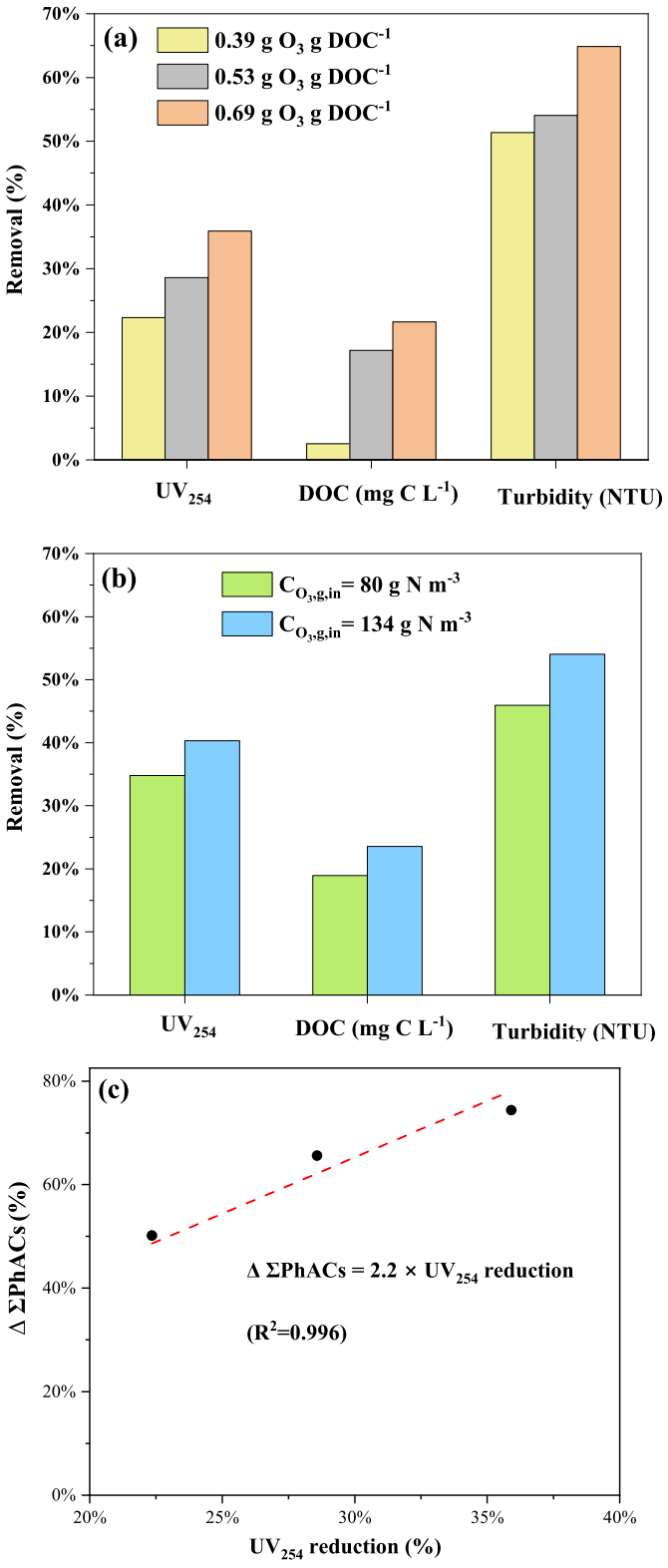

Fig. 5. UV_{254}, DOC, and turbidity removal percentages after ozonation as a function of (a) specific ozone doses (0.39, 0.53, and 0.69 g O_3 g DOC^{-1}), (b) ozone concentration in the inlet gas stream (80 and 134 mg Ndm^{-3}) and (c) correlation between PhACs removal and UV_{254} reduction. For more details on the experimental conditions of each test, see Table 1.

3.3.4. Mass transfer by chemical reaction in the liquid phase

An important dimensionless parameter to take into consideration in gas-liquid mass transfer in the presence of a reaction is the Hatta number (*Ha*). The *Ha* number provides information about the kinetic regimes in a gas-liquid reaction and allows to identify where the chemical reactions take place (Beltrán and Rey, 2018).

For a second-order irreversible reactions, the *Ha* number can be defined by Eq. (14) (Whitman, 1962).

$$\mathrm{Ha} = \frac{\sqrt{k_{O_3} \times D_{O_3} \times C_{P,0}}}{k_L} \tag{14}$$

Where k_{O3} is the kinetic rate constant of ozone with the compound (M^{-1} s^{-1}), $C_{P,0}$ is the initial concentration of PhACs (M), D_{O_3} is the diffusivity of ozone in water (1.76×10^{-9} m^2 s^{-1}) (Johnson and Davis, 1996), and k_L is the liquid phase ozone mass transfer coefficient. The mass transfer coefficient value, $k_L = 4.45 \times 10^{-5}$ m s^{-1}, was determined based on the K_La value obtained under the experimental conditions employed for PhACs ozonation ($Q_G = 0.75$ Ndm^3 min^{-1} and $Q_L = 100$ dm^3 h^{-1}). The *Ha* numbers were only calculated for 11 of the 23 PhACs, i.e., those that were eliminated over 80% with ozonation (for 0.69 g O_3 g DOC^{-1}). Under experimental conditions applied in this study, *Ha* values (see Table S5) were found to be in the range of 0.0002 and 0.17. According to gas-liquid reaction kinetic theory (Charpentier, 1981), *Ha* <0.3 indicates the development of a slow kinetic regime, and most of the reaction occurs in the liquid bulk, i.e., beyond the film. This means that the ozone consumption rate by the PhACs is much slower than the ozone mass transfer from the gas to the liquid phase. Reactors with a large specific interfacial area and high liquid retention time are proper for promoting this type of reaction (Charpentier, 1981). In this study, the membrane contactor provided a large interfacial area, however, the liquid retention time was very short (5.3 s). By increasing the residence time of the aqueous phase in the reactor, would probably have enhanced the interaction between the dissolved ozone and PhACs in the liquid bulk, and thus improving the CECs removal.

Finally, it should be highlighted due to the complexity of the wastewater matrix, other organic/inorganic species present in the sample were not considered in the calculation of *Ha* numbers. Hence, it is possible that these components may also have contributed to an enhancement in the transfer efficiency, as observed in Fig. 4.

4. Conclusions

The findings of this research proved the ability of the tubular porous stainless steel ozone membrane contactor to enhance ozone-liquid mass transfer. The gas and liquid flow rates positively influenced the ozone mass transfer, probably due to an increase in the Reynold number and to the greater mixing induced by the gas stream. Although the mass transfer resistance in the liquid boundary layer was demonstrated to be dominant for low liquid flow rates, and it became almost comparable with membrane resistance for the highest liquid flow rate tested. The volumetric mass transfer coefficient K_La values (1.7–6.1 min^{-1}) proved to be three times greater than the conventional bubble diffusers but are in the same K_La range as the venturi injection systems. A comparison associated with the oxygen transfer into the water, the volumetric SOTR, and the specific SOTE showed that the membrane contactor transferred O_2 mass into the water between one and two orders of magnitude higher per unit of volume height than those in traditional contactors. The significant mass transfer intensification in the membrane contactor makes it an attractive device for practical applications in gas-liquid mass transfer reactions.

The investigated ozone membrane contactor was also applied to eliminate 23 PhACs detected in the secondary-treated wastewater. Under continuous mode operation and residence time of 60 s, 12 out of the 23 PhACs achieved removals higher than 80% for the highest specific ozone dose of 0.69 g O_3 g^{-1} DOC. There was a strong correlation

between micropollutant elimination and k_{O3} and $k_{HO\bullet}$ values, which resulted in a characteristic pattern of elimination for each compound group. Compounds containing carboxylic acid groups, halogen substituents, or amides were highly resistant to ozonation. Regarding global physicochemical parameters, there was no significant mineralization observed at the end of the treatment time under the experimental conditions investigated. However, it is recommended that post-treatment methods such as biological filtration using activated carbon can be employed after ozonation to address the main limitations of this process.

CRediT authorship contribution statement

María A. Prada-Vásquez: Data curation, Formal analysis, Investigation, Methodology, Writing – original draft. **Mateus Mestriner Pituco:** Investigation, Methodology, Writing – review & editing. **Mateus P. Caixeta:** Investigation, Methodology, Writing – review & editing. **Santiago A. Cardona Gallo:** Formal analysis, Investigation, Methodology, Writing – review & editing. **Ana M. Botero-Coy:** Formal analysis, Methodology, Writing – review & editing. **Félix Hernández:** Funding acquisition, Project administration, Resources, Supervision, Validation, Writing – review & editing. **Ricardo A. Torres-Palma:** Supervision, Validation, Writing – review & editing. **Vítor J.P. Vilar:** Conceptualization, Formal analysis, Funding acquisition, Project administration, Resources, Supervision, Validation, Writing – review & editing.

Declaration of competing interest

The authors declare that they have no known competing financial interests or personal relationships that could have influenced the work reported in this paper.

Data availability

Data will be made available on request.

Acknowledgments

This work was financially supported by: Project PTDC/EAM-AMB/4702/2020 - Cutting-Edge Ozone-Technology for Water, with DOI 10.54499/PTDC/EAM-AMB/4702/2020 (https://doi.org/10.54499/PTDC/EAM-AMB/4702/2020); UIDB/50020/2020 and UIDP/50020/2020 (LSRE-LCM), and LA/P/0045/2020 (ALiCE), funded by national funds through FCT/MCTES (PIDDAC). V.J.P. Vilar acknowledges the FCT Individual Call to Scientific Employment Stimulus 2017 (CEECIND/01317/2017). M. Pituco and M. Caixeta acknowledge FCT for their Ph. D. scholarships with references SFRH/BD/144673/2019 and 2020.06681.BD, respectively. Authors from UJI acknowledge Generalitat Valenciana and Ministerio de Ciencia e Innovación for their financial support (Excellence Group Prometeo 2019-040 and Project PID2021-127451OB-I00, respectively). M.A. Prada-Vasquez acknowledge Ministerio de Ciencia Tecnología e Innovación (MINCIENCIAS), Colombia for her PhD fellowship (Convocation 785-2017).

Appendix A. Supplementary data

Supplementary data to this article can be found online at https://doi.org/10.1016/j.chemosphere.2023.140888.

References

Al-Abduly, A., Christensen, P., Harvey, A., Zahng, K., 2014. Characterization and optimization of an oscillatory baffled reactor (OBR) for ozone-water mass transfer. Chem. Eng. Process 84, 82–89. https://doi.org/10.1016/j.cep.2014.03.015.

ASCE, 2007. Measurement of Oxygen Transfer in Clean Water. American Society of Civil Engineers, Reston, USA.

Asghar, A., Lutze, H.V., Tuerk, J., Schmidt, T.C., 2022. Influence of water matrix on the degradation of organic micropollutants by ozone based processes: a review on oxidant scavenging mechanism. J. Hazard Mater. 429, 128189 https://doi.org/10.1016/J.JHAZMAT.2021.128189.

Bader, H., Hoigne, J., 1982. Determination of ozone in water by the indigo method; a submitted standard method. Ozone Sci. Eng. 4, 169–176. https://doi.org/10.1080/01919518208550955.

Bakeri, G., Matsuura, T., Ismail, A.F., Rana, D., 2012. A novel surface modified polyetherimide hollow fiber membrane for gas–liquid contacting processes. Sep. Purif. Technol. 89, 160–170. https://doi.org/10.1016/J.SEPPUR.2012.01.022.

Bamperng, S., Suwannachart, T., Atchariyawut, S., Jiraratananon, R., 2010. Ozonation of dye wastewater by membrane contactor using PVDF and PTFE membranes. Sep. Purif. Technol. 72, 186–193. https://doi.org/10.1016/j.seppur.2010.02.006.

Beltrán, F.J., 2004. Ozone Reaction Kinetics for Water and Wastewater Systems. Lewis Publi., Florida.

Beltrán, F.J., Fernández, L.A., Álvarez, P., Rodriguez, E., 1998. Comparison of ozonation kinetic data from film and Danckwerts theories. Ozone Sci. Eng. 20, 403–420. https://doi.org/10.1080/10874506.01919512.1998.

Beltrán, F.J., Rey, A., 2018. Free radical and direct ozone reaction competition to remove priority and pharmaceutical water contaminants with single and hydrogen peroxide ozonation systems. Ozone Sci. Eng. 40, 251–265. https://doi.org/10.1080/01919512.2018.1431521.

Berry, M.J., Taylor, C.M., King, W., Chew, Y.M.J., Wenk, J., 2017. Modelling of ozone mass-transfer through non-porous membranes for water treatment. Water 9, 452. https://doi.org/10.3390/w9070452.

Botero-Coy, A.M., Martínez-Pachón, D., Boix, C., Rincón, R.J., Castillo, N., Arias-Marín, L.P., Manrique-Losada, L., Torres-Palma, R., Moncayo-Lasso, A., Hernández, F., 2018. 'An investigation into the occurrence and removal of pharmaceuticals in Colombian wastewater.'. Sci. Total Environ. 642, 842–853. https://doi.org/10.1016/j.scitotenv.2018.06.088.

Carvalho, A., Costa, R., Neves, S., Oliveira, C.M., Bettencourt da Silva, R.J.N., 2021. Determination of dissolved oxygen in water by the Winkler method: performance modelling and optimisation for environmental analysis. Microchem. J. 165, 106129 https://doi.org/10.1016/j.microc.2021.106129.

Charpentier, J.C., 1981. Mass-transfer Rates in gas-liquid absorbers and reactors. Adv. Chem. Eng. 11, 1–133. https://doi.org/10.1016/S0065-2377(08)60025-3.

Chys, M., Audenaert, W.T.M., Deniere, E., Mortier, S.T.F.C., Van Langenhove, H., Nopens, I., Demeestere, K., Van Hulle, S.W.H., 2017. Surrogate-based correlation models in view of real-time control of ozonation of secondary treated municipal wastewater - model development and dynamic validation. Environ. Sci. Technol. 51, 14233–14243. https://doi.org/10.1021/acs.est.7b04905.

Dayıoğlu, M.A., 2022. Experimental study on design and operational performance of solar-powered venturi aeration system developed for aquaculture – a semi-floating prototype. Aquac. Eng. 98, 102255 https://doi.org/10.1016/J.AQUAENG.2022.102255.

de Jesus Gaffney, V., Cardoso, V.V., Cardoso, E., Teixeira, A.P., Martins, J., Benoliel, M. J., Almeida, C.M.M., 2017. Occurrence and behaviour of pharmaceutical compounds in a Portuguese wastewater treatment plant: removal efficiency through conventional treatment processes. Environ. Sci. Pollut. Res. 24, 14717–14734. https://doi.org/10.1007/s11356-017-9012-7.

DeMoyer, C.D., Gulliver, J.S., Wilhelms, S.C., 2001. Comparison of submerged aerator effectiveness. Lake Reserv. Manag. 17, 139–152. https://doi.org/10.1080/07438140109353982.

Elovitz, M.S., Von Gunten, U., 1999. Hydroxyl radical/ozone ratios during ozonation processes. I. The R(ct) concept. Ozone Sci. Eng. 21, 239–260. https://doi.org/10.1080/01919519908547239.

Gao, M.T., Hirata, M., Takanashi, H., Hano, T., 2005. Ozone mass transfer in a new gas-liquid contactor-Karman contactor. Sep. Purif. Technol. 42, 145–149. https://doi.org/10.1016/j.seppur.2004.07.004.

Gerrity, D., Gamage, S., Jones, D., Korshin, G.V., Lee, Y., Pisarenko, A., Trenholm, R.A., von Gunten, U., Wert, E.C., Snyder, S.A., 2012. Development of surrogate correlation models to predict trace organic contaminant oxidation and microbial inactivation during ozonation. Water Res. 46, 6257–6272. https://doi.org/10.1016/j.watres.2012.08.037.

Gillot, S., Capela-Marsal, S., Roustan, M., Héduit, A., 2005. Predicting oxygen transfer of fine bubble diffused aeration systems—model issued from dimensional analysis. Water Res. 39, 1379–1387. https://doi.org/10.1016/J.WATRES.2005.01.008.

Gottschalk, C., Libra, J.A., Saupe, A., 2010. Ozonation of Water and Waste Water: a Practical Guide to Understanding Ozone and its Applications, second ed. Wiley-VCH. https://doi.org/10.1002/9783527628926.

Guillossou, R., Le Roux, J., Brosillon, S., Mailler, R., Vulliet, E., Morlay, C., Nauleau, F., Rocher, V., Gaspéri, J., 2020. Benefits of ozonation before activated carbon adsorption for the removal of organic micropollutants from wastewater effluents. Chemosphere 245. https://doi.org/10.1016/j.chemosphere.2019.125530.

Hoigné, J., Bader, H., 1994. Characterization of water quality criteria for ozonation processes. part II: lifetime of added ozone. Ozone. Sci. Eng. 16, 121–134. https://doi.org/10.1080/01919519408552417.

Hollender, J., Zimmermann, S.G., Koepke, S., Krauss, M., Mcardell, C.S., Ort, C., Singer, H., Von Gunten, U., Siegrist, H., 2009. Elimination of organic micropollutants in a municipal wastewater treatment plant upgraded with a full-scale post-ozonation followed by sand filtration. Environ. Sci. Technol. 43, 7862–7869. https://doi.org/10.1021/es9014629.

Hübner, U., von Gunten, U., Jekel, M., 2015. Evaluation of the persistence of transformation products from ozonation of trace organic compounds - a critical review. Water Res. https://doi.org/10.1016/j.watres.2014.09.051.

Iakovides, I.C., Michael-Kordatou, I., Moreira, N.F.F., Ribeiro, A.R., Fernandes, T., Pereira, M.F.R., Nunes, O.C., Manaia, C.M., Silva, A.M.T., Fatta-Kassinos, D., 2019. Continuous ozonation of urban wastewater: removal of antibiotics, antibiotic-

resistant Escherichia coli and antibiotic resistance genes and phytotoxicity. Water Res. 159, 333–347. https://doi.org/10.1016/j.watres.2019.05.025.
Infarmed, 2018. Estatística do medicamento e produtos de saude. URL. https://www.infarmed.pt/web/infarmed/entidades/medicamentos-uso humano/monitorizacao-mercado/estatistica-anual/relatorios-anuais.
Iversen, S.B., Bhatia, V.K., Dam-Johansen, K., Jonsson, G., 1997. Characterization of microporous membranes for use in membrane contactors. J. Memb. Sci. 130, 205–217. https://doi.org/10.1016/S0376-7388(97)00026-4.
John, A., Brookes, A., Carra, I., Jefferson, B., Jarvis, P., 2022. Microbubbles and their application to ozonation in water treatment: a critical review exploring their benefit and future application. Crit. Rev. Environ. Sci. Technol. https://doi.org/10.1080/10643389.2020.1860406.
Johnson, P.N., Davis, R.A., 1996. Diffusivity of ozone in water. J. Chem. Eng. Data 41, 1485–1487. https://doi.org/10.1021/je9602125.
Khaisri, S., DeMontigny, D., Tontiwachwuthikul, P., Jiraratananon, R., 2010. A mathematical model for gas absorption membrane contactors that studies the effect of partially wetted membranes. J. Memb. Sci. 347, 228–239. https://doi.org/10.1016/j.memsci.2009.10.028.
Khaisri, S., DeMontigny, D., Tontiwachwuthikul, P., Jiraratananon, R., 2009. Comparing membrane resistance and absorption performance of three different membranes in a gas absorption membrane contactor. Sep. Purif. Technol. 65, 290–297. https://doi.org/10.1016/j.seppur.2008.10.035.
Kharel, S., Stapf, M., Miehe, U., Ekblad, M., Cimbritz, M., Falås, P., Nilsson, J., Sehlén, R., Bester, K., 2020. Ozone dose dependent formation and removal of ozonation products of pharmaceuticals in pilot and full-scale municipal wastewater treatment plants. Sci. Total Environ. 731 https://doi.org/10.1016/j.scitotenv.2020.139064.
Kreulen, H., Smolders, C.A., Versteeg, G.F., Van Swaaij, W.P.M., 1993. Determination of mass transfer rates in wetted and non-wetted microporous membranes. Chem. Eng. Sci. 48, 2093–2102. https://doi.org/10.1016/0009-2509(93)80084-4.
Kukuzaki, M., Fujimoto, K., Kai, S., Ohe, K., Oshima, T., Baba, Y., 2010. Ozone mass transfer in an ozone-water contacting process with Shirasu porous glass (SPG) membranes-A comparative study of hydrophilic and hydrophobic membranes. Sep. Purif. Technol. 72, 347–356. https://doi.org/10.1016/j.seppur.2010.03.004.
Lado Ribeiro, A.R., Moreira, N.F.F., Li Puma, G., Silva, A.M.T., 2019. Impact of water matrix on the removal of micropollutants by advanced oxidation technologies. Chem. Eng. J. 363, 155–173. https://doi.org/10.1016/j.cej.2019.01.080.
Lee, Y., Von Gunten, U., 2016. Advances in predicting organic contaminant abatement during ozonation of municipal wastewater effluent: reaction kinetics, transformation products, and changes of biological effects. Environ. Sci. Water Res. Technol. https://doi.org/10.1039/c6ew00025h.
Lee, Y., von Gunten, U., 2012. Quantitative structure-activity relationships (QSARs) for the transformation of organic micropollutants during oxidative water treatment. Water Res. https://doi.org/10.1016/j.watres.2012.06.006.
Li, K., Zhang, Y., Xu, L., Liu, L., Wang, Z., Hou, D., Wang, Y., Wang, J., 2020. Mass transfer and interfacial reaction mechanisms in a novel electro-catalytic membrane contactor for wastewater treatment by O3. Appl. Catal., B 264. https://doi.org/10.1016/j.apcatb.2019.118512.
Lopez, F.J., Pitarch, E., Botero-Coy, A.M., Fabregat-Safont, D., Ibáñez, M., Marin, J.M., Peruga, A., Ontañón, N., Martínez-Morcillo, S., Olalla, A., Valcárcel, Y., Varó, I., Hernández, F., 2022. Removal efficiency for emerging contaminants in a WWTP from Madrid (Spain) after secondary and tertiary treatment and environmental impact on the Manzanares River. Sci. Total Environ. 812, 152567 https://doi.org/10.1016/j.scitotenv.2021.152567.
Lu, J.G., Zheng, Y.F., Cheng, M.D., 2008. Wetting mechanism in mass transfer process of hydrophobic membrane gas absorption. J. Memb. Sci. 308, 180–190. https://doi.org/10.1016/J.MEMSCI.2007.09.051.
Marce, M., Domenjoud, B., Esplugas, S., Baig, S., 2016. Ozonation treatment of urban primary and biotreated wastewaters: impacts and modeling. Chem. Eng. J. 283, 768–777. https://doi.org/10.1016/J.CEJ.2015.07.073.
Margot, J., Kienle, C., Magnet, A., Weil, M., Rossi, L., de Alencastro, L.F., Abegglen, C., Thonney, D., Chèvre, N., Schärer, M., Barry, D.A., 2013. Treatment of micropollutants in municipal wastewater: ozone or powdered activated carbon? Sci. Total Environ. 461–462, 480–498. https://doi.org/10.1016/j.scitotenv.2013.05.034.
Mathon, B., Coquery, M., Liu, Z., Penru, Y., Guillon, A., Esperanza, M., Miège, C., Choubert, J.M., 2021. Ozonation of 47 organic micropollutants in secondary treated municipal effluents: direct and indirect kinetic reaction rates and modelling. Chemosphere 262. https://doi.org/10.1016/j.chemosphere.2020.127969.
Mecha, A.C., Onyango, M.S., Ochieng, A., Momba, M.N.B., 2016. Impact of ozonation in removing organic micro-pollutants in primary and secondary municipal wastewater: effect of process parameters. Water Sci. Technol. 74, 756–765. https://doi.org/10.2166/wst.2016.276.
Michael, I., Rizzo, L., McArdell, C.S., Manaia, C.M., Merlin, C., Schwartz, T., Dagot, C., Fatta-Kassinos, D., 2013. Urban wastewater treatment plants as hotspots for the release of antibiotics in the environment: a review. Water Res. https://doi.org/10.1016/j.watres.2012.11.027.
Moreira, F.C., Bocos, E., Faria, A.G.F., Pereira, J.B.L., Fonte, C.P., Santos, R.J., Lopes, J.C.B., Dias, M.M., Sanromán, M.A., Pazos, M., Boaventura, R.A.R., Vilar, V.J.P., 2019. Selecting the best piping arrangement for scaling-up an annular channel reactor: an experimental and computational fluid dynamics study. Sci. Total Environ. 667, 821–832. https://doi.org/10.1016/J.SCITOTENV.2019.02.260.
My Hanh Le, T., Nuisin, R., Mongkolnavin, R., Painmanakul, P., Sairiam, S., 2022. Enhancing dye wastewater treatment efficiency in ozonation membrane contactors by chloro– and fluoro–organosilanes' functionality on hydrophobic PVDF membrane modification. Sep. Purif. Technol. 288, 120711 https://doi.org/10.1016/j.seppur.2022.120711.
Nakada, N., Shinohara, H., Murata, A., Kiri, K., Managaki, S., Sato, N., Takada, H., 2007. Removal of selected pharmaceuticals and personal care products (PPCPs) and endocrine-disrupting chemicals (EDCs) during sand filtration and ozonation at a municipal sewage treatment plant. Water Res. 41, 4373–4382. https://doi.org/10.1016/j.watres.2007.06.038.
Pabby, A.K., Sastre, A.M., 2013. State-of-the-art review on hollow fibre contactor technology and membrane-based extraction processes. J. Memb. Sci. https://doi.org/10.1016/j.memsci.2012.11.060.
Patel, M., Kumar, R., Kishor, K., Mlsna, T., Pittman, C.U., Mohan, D., 2019. Pharmaceuticals of emerging concern in aquatic systems: chemistry, occurrence, effects, and removal methods. Chem. Rev. https://doi.org/10.1021/acs.chemrev.8b00299.
Pines, D.S., Min, K.N., Ergas, S.J., Reckhow, D.A., 2005. Investigation of an ozone membrane contactor system. Ozone Sci. Eng. 27, 209–217. https://doi.org/10.1080/01919510590945750.
Presumido, P.H., Montes, R., Quintana, J.B., Rodil, R., Feliciano, M., Puma, G.L., Gomes, A.I., Vilar, V.J.P., 2022. Ozone membrane contactor to intensify gas/liquid mass transfer and contaminants of emerging concern oxidation. J. Environ. Chem. Eng. 10, 108671 https://doi.org/10.1016/j.jece.2022.108671.
Presumido, P.H., Ribeirinho-Soares, S., Montes, R., Quintana, J.B., Rodil, R., Ribeiro, M., Neuparth, T., Santos, M.M., Feliciano, M., Nunes, O.C., Gomes, A.I., Vilar, V.J.P., 2023. Ozone membrane contactor for tertiary treatment of urban wastewater: chemical, microbial and toxicological assessment. Sci. Total Environ. 164492 https://doi.org/10.1016/J.SCITOTENV.2023.164492.
Rosal, R., Rodríguez, A., Perdigón-Melón, J.A., Mezcua, M., Hernando, M.D., León, P., García-Calvo, E., Agüera, A., Fernández-Alba, A.R., 2008. Removal of pharmaceuticals and kinetics of mineralization by O3/H2O2 in a biotreated municipal wastewater. Water Res. 42, 3719–3728. https://doi.org/10.1016/j.watres.2008.06.008.
Roustan, M., 2003. Transferts gaz-liquide dans les procédés de traitement des eaux et des effluents gazeux. Génie des Procédés de l'Environnement.
Roustan, M., Wang, R.Y., Wolbert, D., 1996. Modeling hydrodynamics and mass transfer parameters in a continuous ozone bubble column. Ozone Sci. Eng. 18, 99–115. https://doi.org/10.1080/01919519608547331.
Sá, M.F.T., Castro, V., Gomes, A.I., Morais, D.F.S., Silva Braga, R.V.P.S., Saraiva, I., Souza-Chaves, B.M., Park, M., Fernández-Fernández, V., Rodil, R., Montes, R., Quintana, J.B., Vilar, V.J.P., 2022. Tracking pollutants in a municipal sewage network impairing the operation of a wastewater treatment plant. Sci. Total Environ. 817, 152518 https://doi.org/10.1016/j.scitotenv.2021.152518.
Sabelfeld, M., Geißen, S.U., 2019. Effect of helical structure on ozone mass transfer in a hollow fiber membrane contactor. J. Memb. Sci. 574, 222–234. https://doi.org/10.1016/j.memsci.2018.10.056.
Samal, K., Mahapatra, S., Hibzur Ali, M., 2022. Pharmaceutical wastewater as Emerging Contaminants (EC): treatment technologies, impact on environment and human health. Energy Nexus 6, 100076. https://doi.org/10.1016/j.nexus.2022.100076.
Santos, L.H.M.L.M., Araújo, A.N., Fachini, A., Pena, A., Delerue-Matos, C., Montenegro, M.C.B.S.M., 2010. Ecotoxicological aspects related to the presence of pharmaceuticals in the aquatic environment. J. Hazard Mater. https://doi.org/10.1016/j.jhazmat.2009.10.100.
Schmitt, A., Mendret, J., Brosillon, S., 2022. Evaluation of an ozone diffusion process using a hollow fiber membrane contactor. Chem. Eng. Res. Des. 177, 291–303. https://doi.org/10.1016/J.CHERD.2021.11.002.
Schmitt, A., Mendret, J., Cheikho, H., Brosillon, S., 2023. Ozone diffusion through a hollow fiber membrane contactor for pharmaceuticals removal and bromate minimization. Membranes 13. https://doi.org/10.3390/membranes13020171.
Sleeper, W., Henry, D., 2002. Durability test results of construction and process materials exposed to liquid and gas phase ozone. Ozone Sci. Eng. 24, 249–260. https://doi.org/10.1080/01919510208901616.
Song, R.B., Xiang, J.Y., Hou, D.P., 2011. Characteristics of mechanical properties and microstructure for 316L austenitic stainless steel. J. Iron Steel Res. Int. 18, 53–59. https://doi.org/10.1016/S1006-706X(11)60117-9.
Sotelo, J.L., Beltrán, F.J., Benitez, F.J., Beltrán-Heredia, J., 1989. Henry's law constant for the ozone-water system. Water Res. 23, 1239–1246. https://doi.org/10.1016/0043-1354(89)90186-3.
Staehelin, J., Holgné, J., 1982. Decomposition of ozone in water: rate of initiation by hydroxide ions and hydrogen peroxide. Environ. Sci. Technol. 16, 676–681. https://doi.org/10.1021/es00104a009.
Stylianou, S.K., Katsoyiannis, I.A., Mitrakas, M., Zouboulis, A.I., 2018. Application of a ceramic membrane contacting process for ozone and peroxone treatment of micropollutant contaminated surface water. J. Hazard Mater. 358, 129–135. https://doi.org/10.1016/j.jhazmat.2018.06.060.
Stylianou, S.K., Sklari, S.D., Zamboulis, D., Zaspalis, V.T., Zouboulis, A.I., 2015. Development of bubble-less ozonation and membrane filtration process for the treatment of contaminated water. J. Memb. Sci. 492, 40–47. https://doi.org/10.1016/j.memsci.2015.05.036.
Therrien, J.D., Vanrolleghem, P.A., Dorea, C.C., 2019. Characterization of the performance of venturi-based aeration devices for use in wastewater treatment in low-resource settings. WaterSA 45, 251–258. https://doi.org/10.4314/WSA.V45I2.12.
Völker, J., Stapf, M., Miehe, U., Wagner, M., 2019. Systematic review of toxicity removal by advanced wastewater treatment technologies via ozonation and activated carbon. Environ. Sci. Technol. https://doi.org/10.1021/acs.est.9b00570.
Wang, B., Xiong, X., Shui, Y., Huang, Z., Tian, K., 2019. A systematic study of enhanced ozone mass transfer for ultrasonic-assisted PTFE hollow fiber membrane aeration process. Chem. Eng. J. 357, 678–688. https://doi.org/10.1016/j.cej.2018.09.188.

Wang, B., Zhang, H., Meng, Q., Ren, H., Xiong, M., Gao, C., Wang, B., 2021. The enhancement of ozone-liquid mass transfer performance in a PTFE hollow fiber membrane contactor using ultrasound as a catalyzer. RSC Adv. 11, 14017–14028. https://doi.org/10.1039/d1ra00452b.

Wang, H., Zhang, S., He, X., Yang, Y., Yang, X., Van Hulle, S.W.H., 2023. Comparison of macro and micro-pollutants abatement from biotreated landfill leachate by single ozonation, O3/H2O2, and catalytic ozonation processes. Chem. Eng. J. 452, 139503 https://doi.org/10.1016/j.cej.2022.139503.

Whitman, W.G., 1962. The two film theory of gas absorption. Int. J. Heat Mass Transf. 5, 429–433. https://doi.org/10.1016/0017-9310(62)90032-7.

Wilke, C.R., Chang, P., 1955. Correlation of diffusion coefficients in dilute solutions. AIChE J. 1, 264–270. https://doi.org/10.1002/AIC.690010222.

Wilson, E.E., 1915. A basis for rational design of heat transfer apparatus. Trans. ASME 37 (47), 47–82. The J. Am. Soc. Mech. Engrs. 53, 1689–1699.

Wittmer, A., Heisele, A., McArdell, C.S., Böhler, M., Longree, P., Siegrist, H., 2015. Decreased UV absorbance as an indicator of micropollutant removal efficiency in wastewater treated with ozone. Water Sci. Technol. 71, 980–985. https://doi.org/10.2166/wst.2015.053.

Zhang, Y., Li, K., Wang, J., Hou, D., Liu, H., 2017. Ozone mass transfer behaviors on physical and chemical absorption for hollow fiber membrane contactors. Water Sci. Technol. 76, 1360–1369. https://doi.org/10.2166/WST.2017.254.

Zimmermann, S.G., Wittenwiler, M., Hollender, J., Krauss, M., Ort, C., Siegrist, H., von Gunten, U., 2011. Kinetic assessment and modeling of an ozonation step for full-scale municipal wastewater treatment: micropollutant oxidation, by-product formation and disinfection. Water Res. 45, 605–617. https://doi.org/10.1016/J.WATRES.2010.07.080.

Zoumpouli, G.A., Baker, R., Taylor, C.M., Chippendale, M.J., Smithers, C., Ho, S.S.X., Mattia, D., Chew, Y.M.J., Wenk, J., 2018. A single tube contactor for testing membrane ozonation. Water 10, 1416. https://doi.org/10.3390/w10101416.